Contents lists available at ScienceDirect

Organic Geochemistry

journal homepage: www.elsevier.com/locate/orggeochem

Superimposed secondary alteration of oil reservoirs. Part I: Influence of biodegradation on the gas generation behavior of crude oils

Yuhong Liao [a,1,*], Weimin Liu [a,b,1], Yinhua Pan [a], Xiaofeng Wang [c], Yunpeng Wang [a], Ping'an Peng [a]

[a] State Key Laboratory of Organic Geochemistry, Guangzhou Institute of Geochemistry, Chinese Academy of Sciences, Guangzhou 510640, PR China
[b] University of Chinese Academy of Sciences, Yuquan Road, Beijing 100049, PR China
[c] State Key Laboratory of Continental Dynamics, Department of Geology, Northwest University, Xi'an 710069, China

ARTICLE INFO

ABSTRACT

Due to multi-stage tectonic movements, many oil reservoirs in typical superimposed basins of China have undergone more than one secondary alteration. Typically, these oil reservoirs experienced biodegradation at an early stage followed by thermal alteration at a later stage. The extent of each secondary alteration can be variable. Here, the succession of biodegradation and subsequent thermal alteration is called superimposed secondary alteration. This study aims not only to show the superimposed secondary alteration process in the reservoir by laboratory simulations, but also to show how varying extents of biodegradation influence the gas generation behavior of crude oils under thermal stress. Hydrocarbon gas generation potential is significantly reduced at the low to moderate biodegradation stage because of the selective removal of normal and branched alkanes. Hydrocarbon gases generated from the more severely biodegraded oils are drier, attributable to the decreasing yields of C_2–C_5 gases relative to methane. In the oil-generative window, the methane generated from more severely biodegraded oils is relatively enriched in ^{13}C. Kinetic modeling suggests that moderately and severely biodegraded oils are thermally less stable than the non-biodegraded and slightly biodegraded oils. The bulk hydrocarbon gas yields from the non-biodegraded oil do not exceed those from the moderately biodegraded oils until EasyRo > 1.6%. For EasyRo of 1.6–2.5%, pyro-bitumen yields from heavily to severely biodegraded oils were about 2–4 times that of non-biodegraded oil. That is, the gas yields normalized to the weight of pyro-bitumen from heavily to severely biodegraded oil is only 25–50% of the gas yield of non-biodegraded oil. Therefore, hydrocarbon gas resource potential based on pyro-bitumen content must be very carefully considered in cases of superimposed secondary alteration.

1. Introduction

Many Cambrian oil reservoirs in the superimposed basins of China (e.g., Sichuan Basin and Tarim Basin) experienced complicated secondary alteration due to multi-stage tectonic movements (Li, 1996; Pang et al., 2010; Zhao et al., 2015). For example, basin uplift and erosion decrease the burial depth of oil reservoirs, resulting in a decrease of reservoir temperature. Biodegradation can occur in the reservoir when the temperature is low enough for microorganisms to survive (Larter et al., 2003, 2006; Aitken et al., 2004; Huang et al., 2004a, 2004b; da Cruz et al., 2011). Subsequently, basin subsidence increases the burial depth and consequently the temperature of oil reservoirs. High temperature can

not only stop biodegradation (Head et al., 2003), but also lead to thermal maturation and/or thermal cracking of reservoir oils (Niu and Hu, 1999; Wang et al., 2006; Zhang et al., 2007a, 2007b; Sun et al., 2009; Tian et al., 2009). The superimposition of biodegradation and thermal alteration has been identified in several petroliferous basins in China. For instance, the Cambrian oil from Tadong-2 well in the Tarim Basin was intensively biodegraded during basin uplift between the Devonian and Permian, forming large amounts of biodegraded oil sands. These oil sands were thermally altered and acted as a secondary hydrocarbon source during basin subsidence at a later stage (Sun et al., 2003; Zhang et al., 2004; Tang and Zan, 2009). Here, the succession of biodegradation and subsequent thermal alteration is described as "superimposed secondary alteration". Such superimposed secondary alteration also occurred in the Central Sichuan Uplift, such as the Anyue gas field. As shown in Fig. 1, the Cambrian oil reservoirs in the Anyue gas field were uplifted-eroded to several hundred meters below the surface dur-
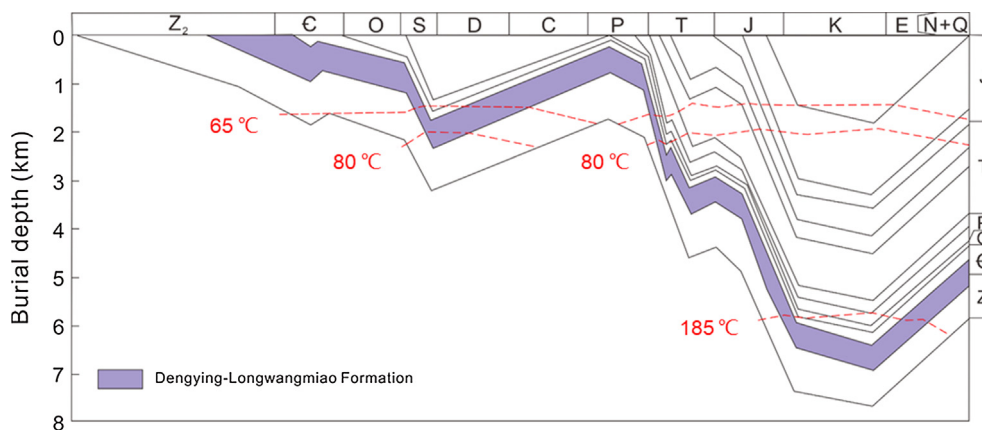
Fig. 1. The reconstructed thermal history of the Moxi-Gaoshiti area in the Sichuan Basin, modified from Zou et al. (2014).

ing the Caledonian tectonic movement (Chen et al., 2011, 2017; Wei et al., 2015; Zhu et al., 2015; Jin et al., 2016). Consequently, the reservoirs cooled to below the zero-biodegradation-rate temperature (80 °C, Head et al., 2003), and were exposed to suitable conditions for biodegradation. Several researchers have provided evidence for early biodegradation in the oil reservoir of the Anyue gas field. For example, Yuan et al. (2009) studied the chromatography of extractable organic matter from drill core solid bitumens of wells Anping-1 and Gaoke-1 of the Anyue gas field and proposed that the initial crude oil charge was biodegraded during reservoir uplift, then the reservoir was charged a second time due to hydrocarbon generation resulting from increasing burial depth. Cheng et al. (2015) further studied the characteristics of adsorbed/occluded hydrocarbons in these solid bitumens and proposed that the reservoir might be charged twice and the initial charge might have experienced slight to moderate biodegradation because the profile of n-alkanes was altered but sterane and hopane distributions remained unaltered. Afterward, the depth of the oil reservoir increased continuously until the mid-Triassic, reaching a maximum burial depth >6000 m and a temperature >185 °C. As a result, the biodegraded oils cracked into hydrocarbon gases (Zou et al., 2014). Similar to the Anyue gas field, previous studies have suggested that the formation of the Weiyuan gas reservoirs was partly attributed to the cracking of Cambrian oil reservoirs that were severely biodegraded during the Caledonian tectonic movement (Wei et al., 2008, 2015; Zou et al., 2014; Shi et al., 2017).

In-reservoir biodegradation can alter the chemical composition of crude oil to varying extents by the selective removal and preservation of various compound classes (Volkman et al., 1984; Huang et al., 2003, 2004; Larter et al., 2003; Aitken et al., 2004; Chang et al., 2018). For example, hydrogen-rich n-alkanes are usually preferentially removed during biodegradation, resulting in the accumulation of compounds depleted in hydrogen (Volkman et al., 1984; Leahy and Colwell, 1990; Aitken et al., 2004; Wentzel et al., 2007). Such variations lead to the alteration of SARA (i.e., saturates, aromatics, resins and asphaltenes) contents of crude oil, causing the decrease of saturates concomitant with a relative enrichment of heavy fractions (resins and asphaltenes) (Volkman et al., 1984; Leahy and Colwell, 1990; Aitken et al., 2004; Wentzel et al., 2007). Additionally, biodegradation can also alter the molecular structures of asphaltenes, especially the hydrogen-rich alkyl moieties (Jenisch-Anton et al., 2000). For example, n-fatty acids and n-alcohols bound to the asphaltene core by relatively weak ester and hydrogen bonds can be removed at slight to moderate biodegradation stages (Pan et al., 2015).

Thermal cracking of crude oil involves various chemical reactions such as defunctionalization, polymerization and condensation (Behar et al., 1992, 1999; Hill et al., 2003). In this way, the thermal cracking behavior of crude oil, such as gas generation potential and thermal stability, is closely related to its chemical composition (Schenk et al., 1997; Behar et al., 1999; Burklé-Vitzthum et al., 2011; Tian et al., 2012). For example, Zhang et al. (a, b) indicated that a precursor oil of higher atomic H/C can generate more hydrocarbon gases under thermal stress. Wang et al. (2010) suggested that the maximum methane yield from the cracking of a Tarim crude oil is much higher than that of the corresponding asphaltene fraction. Tian et al. (2012) also suggested that although the C_1–C_5 gas yields from the aromatics and asphaltenes are lower than those from the saturates and whole crude oil at high thermal maturity level (EasyRo > 2.25%). Hydrocarbon gas generation from the aromatics and asphaltenes starts earlier than from the saturates and crude oil.

Since in-reservoir biodegradation can alter the chemical compositions of crude oil, it may influence the gas generation behavior of the crude oil to some extent. However, such influences have not been systematically studied so far. A lack of knowledge about such influences may cause deviations in hydrocarbon gas generation potential evaluation based on pyrobitumen content, degree of oil transformation, and perhaps gas–source correlation in exploring superimposed petroliferous basins. In this work, a sequence of crude oil and biodegraded tar sands that are of identical origin but at different biodegradation stages (from non-biodegraded to severely biodegraded) was collected from the Liaohe Basin of China. The crude oil and tar sand bitumens were pyrolyzed in a closed system to evaluate how varying degrees of biodegradation can influence oil thermal stability, hydrocarbon gas composition, hydrocarbon gas carbon isotopic compositions, and hydrocarbon gas generation potential/resource evaluation based on pyrobitumen content. Kinetic modeling was employed to extrapolate the influence of biodegradation on the hydrocarbon gas generation behaviors under geological conditions. The influence of biodegradation on hydrocarbon gas resource evaluation based on pyrobitumen content was also explored.

2. Samples and experimental methods

2.1. Samples and pretreatment

Crude oil and bitumens (tar sands from reservoir core) were collected from the Western Depression of the Liaohe Basin in northeast China. The crude oil and the tar sand bitumens were generated from the same source rocks having similar thermal maturities (Lu et al., 1990). The crude oil was non-biodegraded, while the tar sand bitumens suffered varying degrees of biodegra-

dation in the range of 2–8 on the Peters and Moldowan scale (abbreviated as PM level in the following text; Peters et al., 2005). The tar sands were extracted by the procedure described in Liao et al. (2012). In brief, each tar sand was finely crushed and was then added to 50 mL of a dichloromethane:methanol (93:7, v/v) mixture in a 200 mL glass vial. The vial was sealed and sonicated for 30 min. The solids were separated by centrifugation, and the bitumen was transferred to a clean vial where most of the solvent was evaporated under nitrogen. The crude oil sample was also treated using the same method to avoid possible deviations caused by the pretreatment. The biodegraded oils/bitumens were separated into maltene and asphaltene fractions using a deasphalting procedure described in detail by Liao et al. (2009). The maltene fraction was fractionated into saturates, aromatics, and resins using silica gel: alumina column chromatography, eluting with *n*-hexane, DCM:*n*-hexane (3:1, v/v), and DCM:methanol (2:1, v/v), respectively. The oil and bitumens were coded according to their biodegradation levels on the PM scale. For example, the non-biodegraded oil was coded as L-0, and the bitumen of PM level 2 was coded as L-2. Geochemical properties of these crude oil and extracted bitumens are shown in Table 1.

2.2. Pyrolysis experiments and compositional analysis

The crude oil and the tar sand bitumens (10–40 mg) were loaded into gold tubes (40 mm × 5 mm i.d.) with one end prewelded. The tubes were sealed under an argon atmosphere after being purged with argon for 15 min. The sealed tubes were placed in stainless steel autoclaves in an oven. The pyrolysis experiments were conducted under the constant pressure of 50 MPa and the oven was then heated from room temperature to the starting temperature 250 °C at a heating rate of 20 °C/h. Then the oven was separately heated at heating rates of 20 °C/h and 2 °C/h, with 12 sampling temperature points between 300 °C and 600 °C for each heating rate (Table 2). Each autoclave was taken out from the oven and was quickly quenched in cold water when the designated temperature point was reached. During the experiments, the temperature error was less than 1 °C, and the pressure error was less than 2 MPa.

Gold tubes were carefully cleaned before the analysis of gaseous pyrolytic products. The cleaned gold tube was placed in a vacuum line and was pierced with a needle, allowing the gas to escape into the line. Molecular characterization and quantification of the total gas fraction were performed using an Agilent 7890B gas chromatograph equipped with two thermal conductivity detectors (TCD) for the analysis of permanent gases and a flame ionization detector (FID) for hydrocarbon gases. The GC oven temperature was initially held at 60 °C for 3 min, ramped from 60 °C to 190 °C at 25 °C/min, and then held at 190 °C for 3 min. The external standard method was applied in the quantification of gas components.

The yields of solid bitumen were obtained using the method in Xiong et al. (2016). In brief, toluene was used to wash the pyrolytic residue to remove any soluble components. Then the pyrolytic residue was dried and weighed.

Table 2

Sampling temperature points at each heating rate and the corresponding equivalent vitrinite reflectance (EasyRo).

Heating rates (°C/h)	Sampling temperature (°C)	EasyRo[a] (%)
20	330.3	0.55
	354.8	0.66
	376.2	0.75
	402.0	0.91
	426.0	1.13
	451.3	1.41
	473.5	1.71
	497.8	2.09
	521.6	2.50
	546.0	2.95
	569.7	3.39
	594.0	3.79
2	328.7	0.69
	353.0	0.82
	377.1	1.01
	401.3	1.28
	424.8	1.58
	449.4	1.97
	473.6	2.40
	497.9	2.87
	521.4	3.33
	545.8	3.76
	569.1	4.10
	593.6	

[a] EasyRo is calculated using the method in Sweeney and Burnham (1990).

2.3. GC–MS and GC-FID analysis

The saturates of oil and bitumens were analyzed using gas chromatography–mass spectrometry (GC–MS) using a Thermo Scientific Trace GC Ultra gas chromatograph coupled with a Thermo Scientific Trace DSQ II mass spectrometer. An HP-1 fused silica capillary column (30 m × 0.25 mm i.d. × 0.25 μm film thickness) was used. The column was held at 40 °C for 2 min and then ramped to 290 °C at a rate of 4 °C/min with a final hold time of 20 min. Helium was used as the carrier gas at a constant flow rate of 1.2 mL/min. The ion source was maintained at 260 °C and operated in the electron ionization (EI) mode with an electron beam energy of 70 eV. The mass range was set to *m/z* 50–650, and the scan cycle was set to 100 ms.

Due to very good linearity of a flame ionization detector, GC-FID was used to quantify the compositions of liquid pyrolysis product and $C_{15}D_{32}$ was added as an internal standard. GC-FID analysis was performed using an Agilent 7890A gas chromatograph equipped with a flame ionization detector (FID). A DB-5 fused silica capillary column (60 m × 0.32 mm i.d. × 0.25 μm film thickness) was used. The column was held at 35 °C for 2 min and then ramped to 50 °C at a rate of 1.5 °C/min and then ramped to 290 °C at a rate of 4 °C/min with a final hold time of 20 min.

Carbon isotopes of gas components were measured using a Delta plus XL GC–IRMS. Samples were analyzed at least in duplicate with errors less than ± 0.5‰. A Poraplot Q capillary column (30 m × 0.32 mm i.d. × 0.25 μm film thickness) was used. The GC oven temperature was initially held at 50 °C for 3 min, ramped

Table 1

Properties of Liaohe crude oil and extracted bitumen.

Sample	$\delta^{13}C$ (‰)	Biodegradation scale	SARA (wt%)				Biomarker parameters			
			Sat.	Aro.	Res.	Asph.	H_{30}/TT_{23}	$C_{27}RS/S_{22}$	$C_{28}RS/S_{22}$	$C_{29}RS/S_{22}$
L-0	−29.2	0	60.9	14.4	20.2	4.5	50.2	17.8	32.3	35.4
L-2	−29.4	2–3	41.5	13.3	33.8	11.3	42.3	16.7	26.4	33.2
L-5	−30.2	5–6	26.6	14.6	42.4	16.5	34.8	5.9	7.8	11.2
L-8	−30.0	8	18.8	11.8	40.3	29.0	11.1	0.4	1.3	3.4

from 50 °C to 180 °C at 15 °C/min, and then held at 180 °C for 15 min. A working standard of CO_2 gas calibrated against NIST RM-22 (graphite) were employed to calibrate the isotopic ratios. All carbon isotopic ratios were reported in per mil (‰) relative to the VPDB standard.

2.4. Calculation of kinetic parameters

Chemical reactions with different orders may be involved in the thermal cracking of crude oils leading to complex reaction kinetics. Nevertheless, laboratory and empirical data suggest that the thermal cracking of crude oils could be approximately described by a parallel first-order reaction scheme (e.g., Behar et al., 1992, 1997; Hill et al., 2003; Wang et al., 2010; Tian et al., 2012). In this study, the kinetic parameters for gas generation were calculated using the software Kinetics 2000 based on the pyrolysis data of the crude oil and bitumen extracts at two different heating rates (i.e., 20 °C/h and 2 °C/h). A fixed frequency factor ($A = 1.0 \times 10^{-14} \, s^{-1}$) and a discrete distribution of activation energies (1 Kcal spacing) were adopted in the modeling.

3. Results

3.1. Geochemical properties of crude oil and biodegraded bitumens

The crude oil and the bitumen extracts that have suffered different levels of biodegradation vary significantly in their relative SARA contents (Table 1). L-0 is characterized by a high content of saturates (60.9%) with an intact distribution of n-alkanes ranging from C_{11} to C_{37} (Fig. 2). With increasing biodegradation, the relative abundance of the saturates decreased, while the asphaltenes and resins were relatively increased (Table 1). Such a decrease may be attributed to the preferential removal of normal and branched alkanes in the saturates during biodegradation. As shown in Fig. 2, these hydrogen-rich hydrocarbons were significantly removed in L-2 and were exhausted in L-5 and L-8. As a result, C_{30} $17\alpha(H),21\beta(H)$hopane, which is relatively depleted in hydrogen content, became relatively enriched in the TIC (total ion current) chromatograms of those biodegraded bitumens. The rapid removal of normal and branched alkanes during biodegradation is not surprising, as it is well known that they are susceptible to biodegradation, even at an early stage, due to effective strategies by microorganism communities that involve specialized enzyme systems and metabolic pathways (Setti et al., 1993; Cubitto et al., 2004; Zhang et al., 2011). The saturates of L-5 and L-8 differ mainly in the distributions of steranes and terpanes. C_{27-29} regular steranes were largely removed in L-5 and were almost depleted in L-8. C_{30} $17\alpha(H),21\beta(H)$-hopane is more resistant to biodegradation than C_{27-29} regular steranes and became partially degraded in L-8. The C_{22} sterane (S22) and C_{23} tricyclic terpane (TT23) are even more recalcitrant, as is shown by the decreasing ratio of H_{30}/TT_{23} and $C_{27-29}RS/S_{22}$ with increasing biodegradation extents (Table 1).

### 3.2. Evolution of soluble hydrocarbons and solid bitumens during pyrolysis

TICs of soluble hydrocarbons in the liquid pyrolysis products at various pyrolysis temperatures at the heating rate of 2 °C/h are shown in Fig. 3. Light hydrocarbons (C_6–C_{13}) are susceptible to biodegradation and they were only present in L-0 before pyrolysis (Fig. 4a,d). During pyrolysis, light hydrocarbons were generated from cracking of heavy components, while simultaneously, they can also crack into smaller molecules such as wet gases (Hill et al., 2003). As a result, the yields of light hydrocarbons increased first with temperature when the generation rates are higher than the cracking rates and then decreased at higher temperatures when the cracking rates exceeded the generation rates. At the same heating rates, the light hydrocarbon yields of the four samples reached a maximum at similar temperatures. The maximum light hydrocarbon yields from L-5 and L-8 are similar but they are both lower than those from L-0 and L-2. In contrast to the variation trends of light hydrocarbons, the heavy hydrocarbon (C_{14+}) yields of all the four samples continuously decreased with increasing temperatures (Fig. 4b,e). The most significant removal of heavy hydrocarbons occurs in temperature range of 426–451 °C in the experimental run at 20 °C/h while it occurs at 401–425 °C in the experimental run at 2 °C/h, which corresponds to EasyRo range of about 1.1–1.6% (Table 2). Furthermore, at the upper limit of the EasyRo range 1.1–1.6%, the light hydrocarbon yields for all four samples reach their maximum, accompanied by a sharp decrease in C_{14+} yields (Fig. 4). Such consistency may suggest that the light hydrocarbons generated during pyrolysis can at least be partly attributed to the cracking of heavy hydrocarbons. Light hydrocarbons are volatile and hard to quantify accurately. Their yields during pyrolysis may be underestimated, especially within the EasyRo range of about 1.1–1.6% when large amounts of light hydrocarbons were formed by the significant cracking of heavy hydrocarbons.
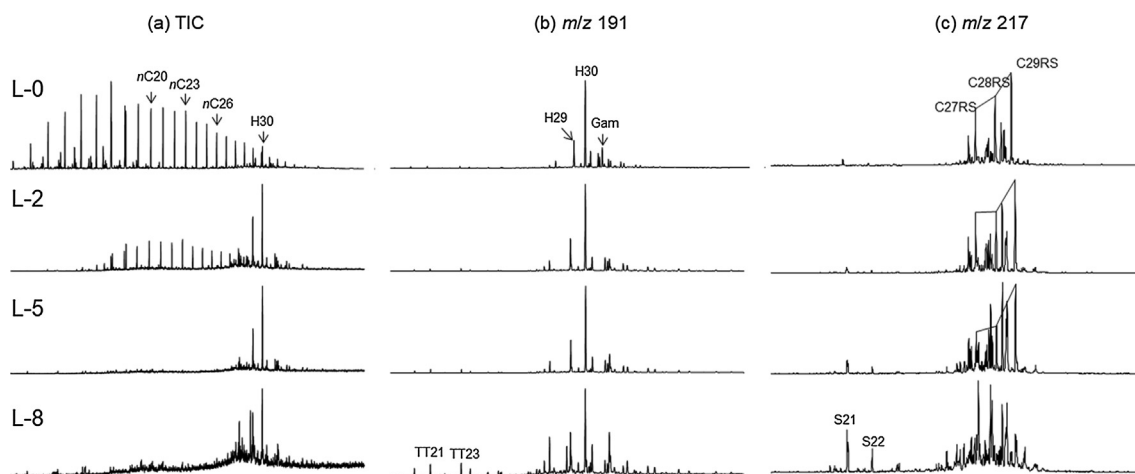
Fig. 2. GC–MS mass chromatograms of (a) TIC, (b) m/z 191, displaying terpanes and (c) m/z 217, displaying steranes in crude oil and extracted bitumens. nC20 = n-eicosane; nC23 = n-tricosane; nC26 = n-hexacosane; H29–30 = C_{29}–C_{30} $17\alpha(H), 21\beta(H)$-hopanes; Gam = gammacerane; C27RS = C_{27} $\alpha\alpha\alpha20R$-cholestane; C28RS = C_{28} $\alpha\alpha\alpha20R$-methylcholestane; C29RS = C_{29} $\alpha\alpha\alpha20R$-ethylcholestane; TT21–23 = C_{21}–C_{23} tricyclic terpanes; S21 = C_{21} sterane; S22 = C_{22} sterane.
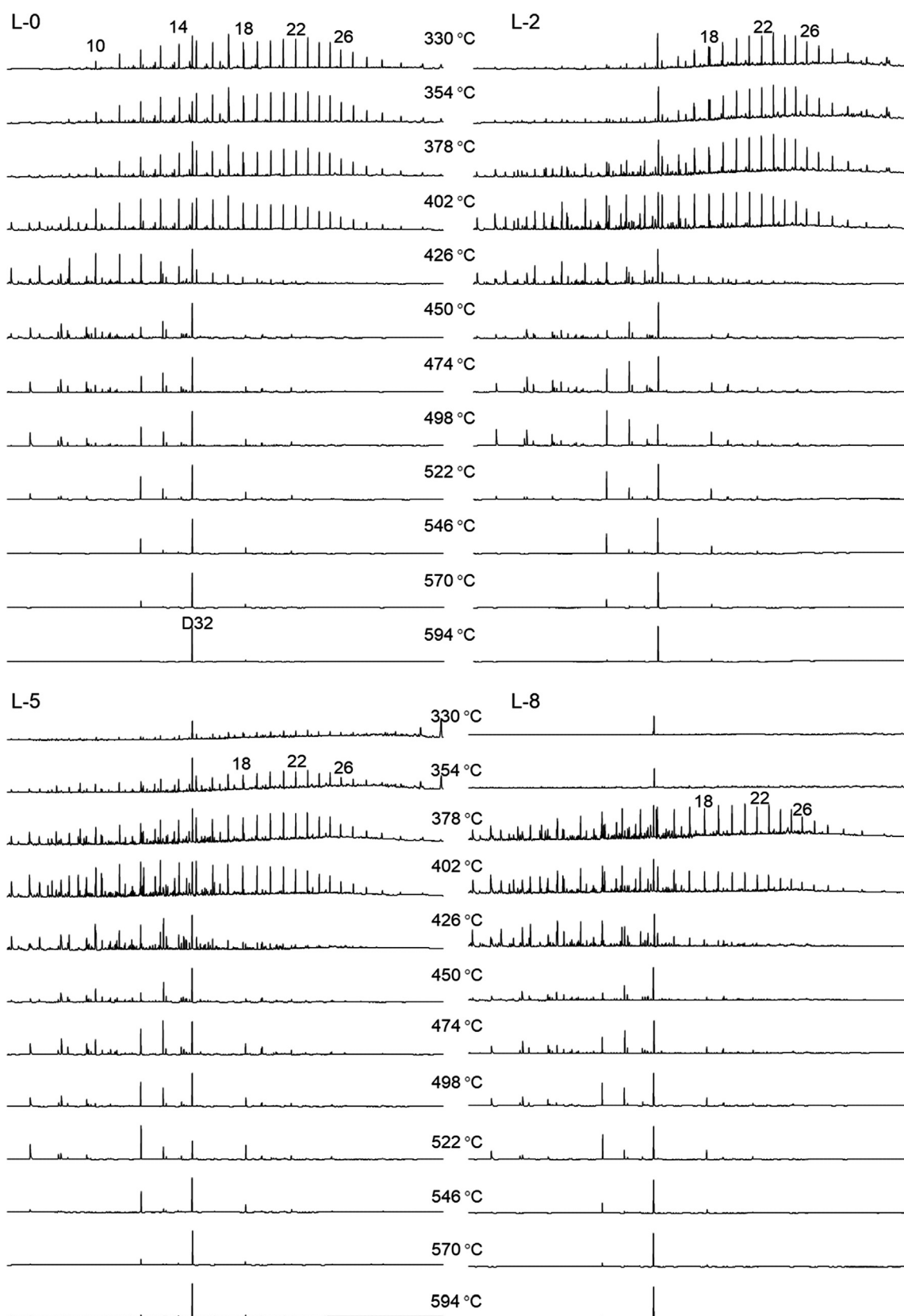
Fig. 3. Total ion chromatograms of the four samples and their products with various pyrolysis temperature at a heating rate of 2 °C/h. Numbers on the peaks refer to carbon number of *n*-alkanes.
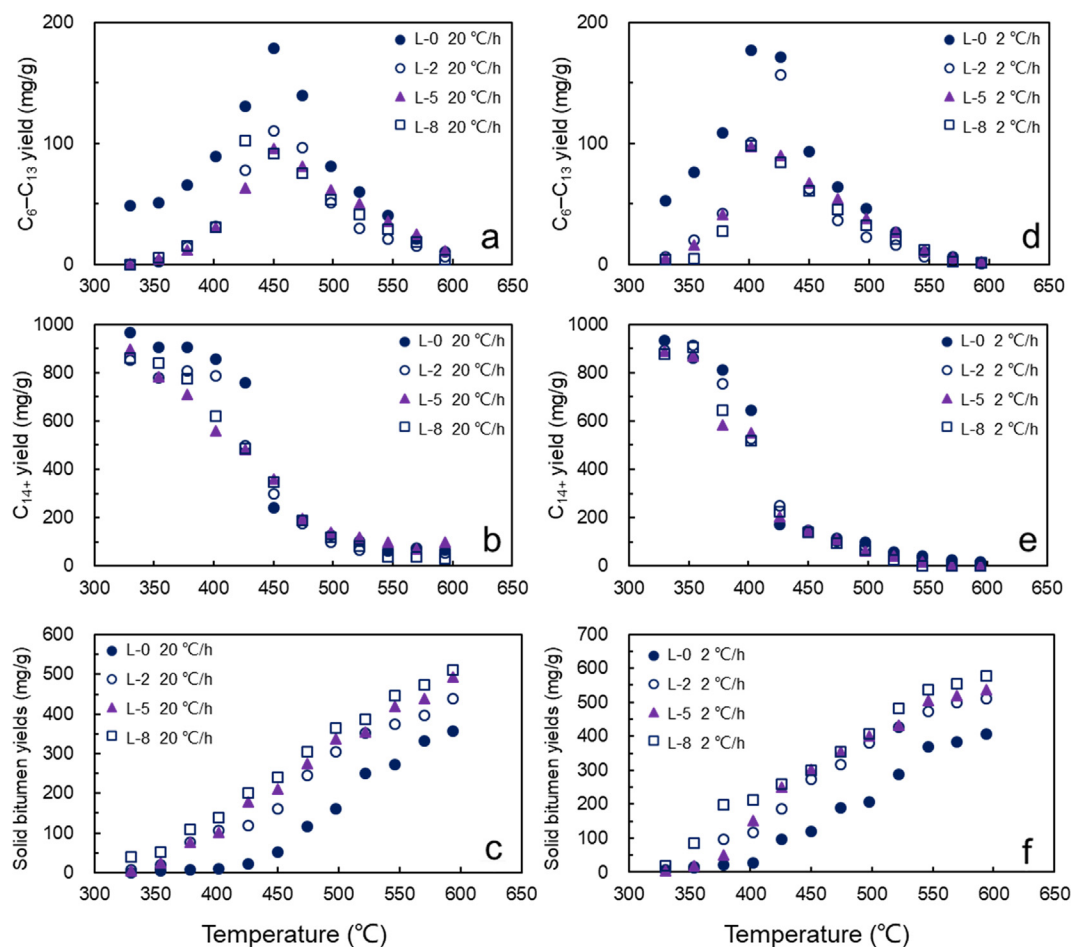
Fig. 4. Pyrolysis results for Liaohe oil and tar sand bitumens showing the yields of: (a) light hydrocarbons (C_6–C_{13}) at a heating rate of 20 °C/h; (b) heavy hydrocarbons (C_{14+}) yields at a heating rate of 20 °C/h; (c) solid bitumen yields at a heating rate of 20 °C/h; (d) light hydrocarbons (C_6–C_{13}) at a heating rate of 2 °C/h; (e) heavy hydrocarbons (C_{14+}) yields at a heating rate of 2 °C/h; (f) solid bitumen yields at a heating rate of 2 °C/h.

In contrast to the variation trends of soluble hydrocarbons, the solid bitumen yields from the four samples continually increased with pyrolysis temperatures (Fig. 4c,f). The solid bitumen yield from the non-biodegraded oil is much lower than those from the biodegraded bitumens throughout the pyrolysis. For example, at the maximum thermal maturity level obtained in the pyrolysis (i.e., 594 °C the heating rate of 2 °C/h), the yield of solid bitumen from L-8 was 577 mg/g, whereas the solid bitumen yield from L-0 was only 406 mg/g. At the same thermal maturity, the solid bitumen yields increase with biodegradation severity. This is consistent with the observation by Connan et al. (1975). They found that, under thermal stress, solid bitumen generation from a biodegraded Swiss oil is faster than from a non-biodegraded oil. Connan et al. (1975) attribute such differences to the relative enrichment of polycyclic alkanes in biodegraded oils, which are more likely to convert to aromatics and form pyrobitumen.

3.3. Hydrocarbon gases

Hydrocarbon gas yields from the four samples are shown in Fig. 5. Methane shows the highest thermal stability among the gaseous hydrocarbons. It accumulates continuously with increasing temperature and it dominates the hydrocarbon gas yields at the maximum thermal maturity level achieved in the pyrolysis (Fig. 5a,e). The final methane yields of the four samples are differ-

ent. L-0 shows the highest final methane yield of the four samples (517 mg/g), while L-8 shows the lowest final methane yield. The final methane yield declines with increasing biodegradation extent. The decline in final methane yields is most significant between L-0 and L-2, while the decline becomes least between L-5 and L-8. Nevertheless, it is notable that L-5 and L-8 produced slightly more methane than L-0 below EasyRo% value of 2.1% (before 498 °C for 20 °C/h).

In contrast to the continual increase of methane, the yield of ethane rises first and then falls due to severe secondary cracking at high temperature (Fig. 5b,f). The temperature of maximum ethane yield is similar for the four samples. They are around 546 °C for the four samples heated at 20 °C/h, and around 498 °C in the experimental runs at 2 °C/h, with the EasyRo value of about 2.9%. The L-0 sample maximum ethane yield of sample L-0 is 208 mg/g, while the ethane yields from biodegraded bitumens are much lower.

In the same experimental run, the maximum yields of C_3 and C_4–C_5 gases are lower than the maximum ethane yields, and their maximum temperatures are lower than those of ethane (Fig. 5c,d,g, h). The respective maximum temperatures of propane are about 498 °C and 474 °C for the four samples heated at 20 °C/h and 2 °C/h, respectively, and those of C_4–C_5 gases shift to 474 °C for the 20 °C/h run and 449 °C for the 2 °C/h run. The maximum C_3 and C_4–C_5 gas yields from the non-biodegraded L-0 are both higher than those from the biodegraded bitumens.
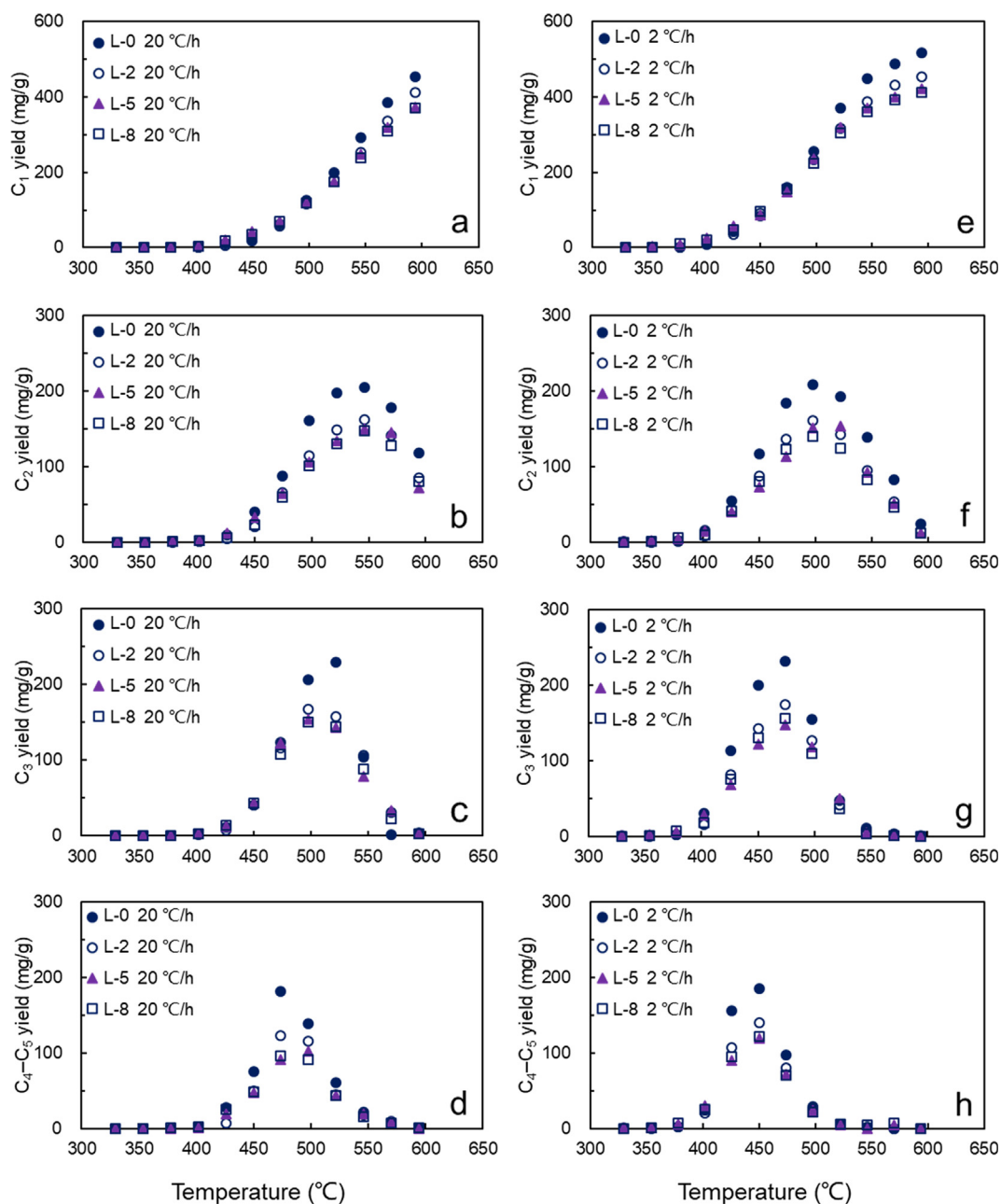
Fig. 5. Pyrolysis results for Liaohe oil and tar sand bitumens showing the yields of: (a) methane yields at a heating rate of 20 °C/h; (b) ethane yields at a heating rate of 20 °C/h; (c) propane yields at a heating rate of 20 °C/h; (d) C_4–C_5 yields at a heating rate of 20 °C/h; (e) methane yields at a heating rate of 2 °C/h; (f) ethane yields at a heating rate of 2 °C/h; (g) propane yields at a heating rate of 2 °C/h; (h) C_4–C_5 yields at a heating rate of 2 °C/h.

3.4. Stable carbon isotopes of hydrocarbon gases

The bulk carbon isotopic compositions of the original oil and bitumen samples are rather close, with more severely biodegraded oils being slightly enriched in ^{12}C (Table 1). Fig. 6a,d shows a comparison of the stable carbon isotopic compositions of methane generated from the four samples during pyrolysis. With the pyrolysis temperature lower than 355 °C for the 20 °C/h run and 329 °C for the 2 °C/h run, L-0 did not produce sufficient hydrocarbon gases for the accurate measurement of stable carbon isotopic composition. It is notable that in the oil-generative window methane generated from more severely biodegraded oils is generally more enriched in ^{13}C than methane from the less severely biodegraded oils. For example, at the heating rate of 20 °C/h, the measured

methane carbon isotope at 376 °C for the non-biodegraded oil L-0 is −58.8‰, while the measured methane carbon isotope at 376 °C for the severely biodegraded oil L-8 is −42.7‰. Such differences become smaller with increasing thermal stress. At the maximum thermal maturity level obtained in this study, the measured methane carbon isotope for the non-biodegraded oil L-0 is −35.3‰, while the measured methane carbon isotope for the severely biodegraded oil L-8 is −35.7‰, the differences among all these samples are negligible.

Fig. 6b–f shows the stable carbon isotopic compositions of ethane and propane generated from the four samples during pyrolysis. Compared to methane, there are smaller differences in the stable carbon isotopic compositions of ethane and propane generated from the four samples throughout the pyrolysis. Ethane from
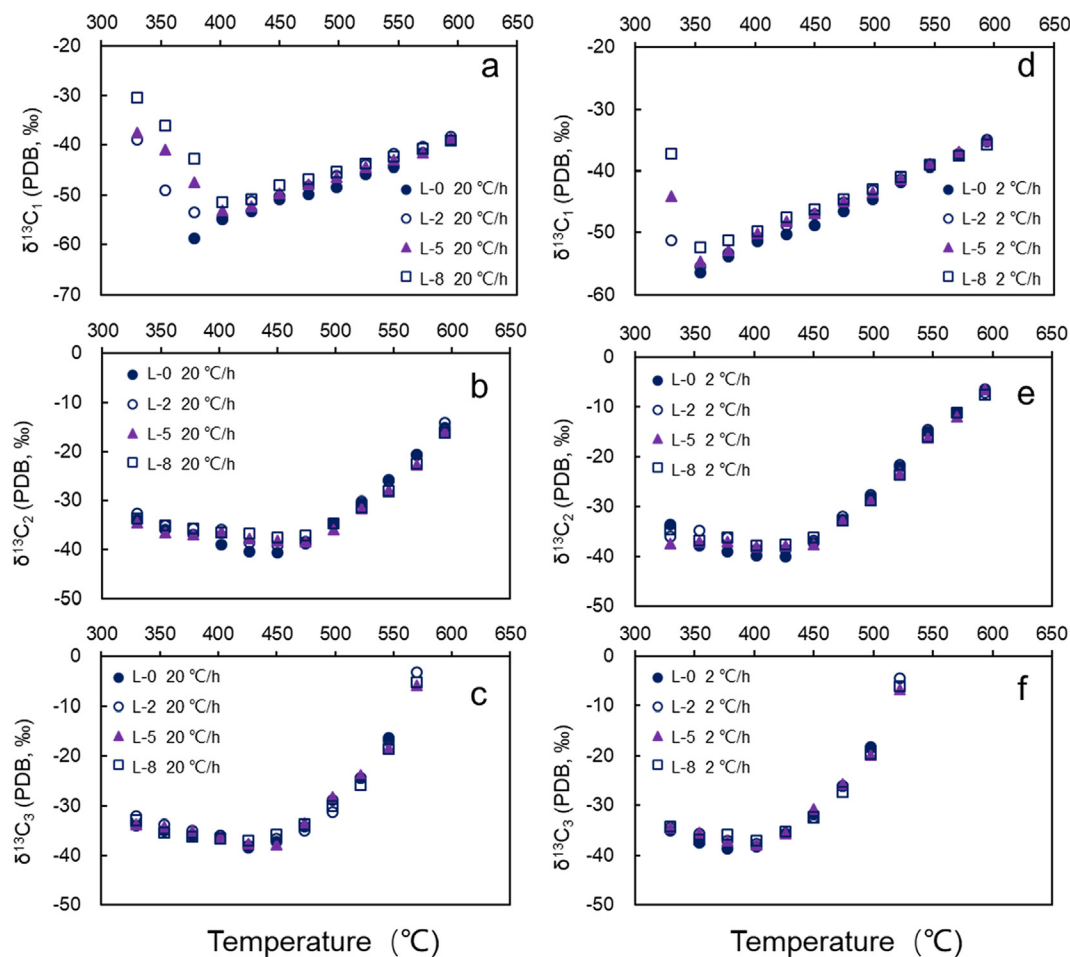
Fig. 6. Evolution trends of carbon isotopic compositions of: (a) methane at a heating rate of 20 °C/h; (b) ethane at a heating rate of 20 °C/h; (c) propane at a heating rate of 20 °C/h; (d) methane at heating rate of 2 °C/h; (e) ethane at a heating rate of 2 °C/h; (f) propane at a heating rate of 2 °C/h.

more severely biodegraded oils was somewhat enriched in ^{13}C (up to 3.2‰ less negative $\delta^{13}C$ values). Moreover, ethane and propane generated from the four samples show similar thermal evolution trends. They all initially become enriched in ^{12}C and then become enriched in ^{13}C with increasing thermal stress.

4. Discussion

4.1. Hydrocarbon gas generation potential and its correlation with solid bitumen yields

The results above suggest that crude oils with varying biodegradation extents can have differences in the gas generation behavior under thermal stress. With increasing biodegradation extent, the final hydrocarbon gas yields decreased, along with the decrease of saturates and the increase of resins and asphaltenes (Fig. 7). This suggests that the preferential removal of hydrogen-rich components during biodegradation reduced the gas generation potential of crude oils. Moreover, such reduction in the gas generation potential is more significant at the early biodegradation stages, where normal and branched alkanes were preferentially removed (Fig. 2). By comparison, the decrease in the hydrocarbon gas generation potential between moderate and severe biodegradation stages is not very significant. The cracking of oil to gas in a closed system is, in fact, a hydrogen redistribution process, resulting in the formation of hydrogen-enriched hydrocarbon gases and hydrogen-depleted solid bitumen (Hill et al., 2003; Behar et al.,
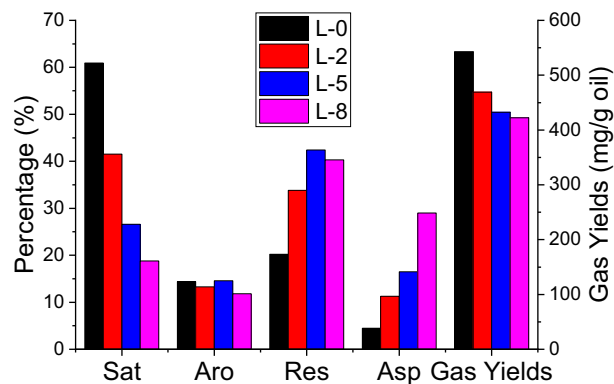
Fig. 7. Distributions of SARA fractions and the final gas yields of Liaohe oil and bitumens.

2008; Fusetti et al., 2010). The amount of hydrogen available controls the final hydrocarbon gas yields under severe thermal stress (Hill et al., 2003; Tian et al., 2009). Normal and branched alkanes are the most hydrogen-rich oil components (H = 2n + 2, where n is the number of carbon atoms). The progressive removal of normal and branched alkanes from the biodegraded bitumens is responsible for the decrease in hydrocarbon gas generation potential in this study (Fig. 8). Moreover, different precursor oils usually have different abundances of alkane. Our results imply that, at the same
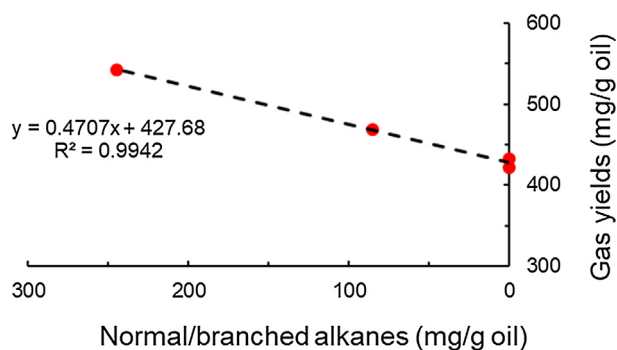
Fig. 8. Linear regression of the concentration of normal/branched alkanes and the hydrocarbon gas yields (by weight) of the samples.

biodegradation stage, the decreases in the hydrocarbon gas generation potential of precursor oils with more abundant alkanes could be more significant than those with less abundant alkanes.

Fatty acids are one common biodegradation product of normal and branched alkanes (Aitken et al., 2004; Dutta, 2005; Liu et al., 2018). These fatty acids could also progressively be consumed with increasing biodegradation severity as shown in Liao et al. (2012). That is, both the alkanes and their biodegradation products could be progressively removed from the crude oil during biodegradation at low to moderate biodegradation. By comparison, the biodegradation of more complex saturated hydrocarbons may follow different pathways. For example, hopanes were altered at the severe biodegradation stage (L-8) in this study. However, the direct attack on the saturated ring structure of hopanes is rarely seen. Instead, hopanes may be degraded via demethylation to form norhopanes (Moldowan and McCaffrey, 1995; Frontera-Suau et al., 2002; Pan et al., 2017b) or via β-oxidation of the alkyl side chain to form hopanoic acids (Watson et al., 2002; Liao et al., 2012). In addition to hopanes, tricyclic terpanes were also proposed to be biodegraded via the alteration of alkyl side chains, resulting in the formation of nor-tricyclic terpanes (Cheng et al., 2016). Therefore, between moderate and severe biodegradation stages, the hydrogen content of a crude oil is not significantly influenced by microorganisms. As a result, the hydrocarbon gas generation potential of biodegraded oil does not change very much between moderate and severe biodegradation stages.

Furthermore, asphaltenes can also be thermally degraded to generate hydrocarbon gases. For example, Wang et al. (2010) reported a maximum of about 400 mg/g hydrocarbon gas yields from asphaltene pyrolysis, while Tian et al. (2012) reported a maximum of around 250 mg/g hydrocarbon gas yields from asphaltene pyrolysis. Calemma and Rausa (1997) suggested that the final gas yields from asphaltene pyrolysis depend linearly on the aliphatic carbon fraction of the asphaltenes. Supplementary Fig. S1 shows the compositions of C_1–C_5 alkyl moieties within the asphaltene molecular structure characterized by on-line quantitative flash pyrolysis-gas chromatography coupled with FID (Py-GC-FID) in a method similar to Liao et al. (2015) and Pan et al. (2015). Combined with the Py-GC-FID results in Pan et al. (2015), the quantitative variations of aliphatic carbon fraction within asphaltenes during biodegradation could be obtained (Supplementary Fig. S2). These results suggest that there is only a slight decrease in the aliphatic carbon fraction within the asphaltenes over the PM level range of 2–8 (~6.13 mg/g asphaltenes). Therefore, the hydrocarbon gas generation potential of the asphaltenes was not significantly altered by biodegradation. However, the asphaltene secondary gas should become a more important constituent of the secondary gas from more severely biodegraded oils due to the progressive enrichment of asphaltenes (Table 1).

In addition to the decrease in hydrocarbon gas yield resulting from biodegradation, the absolute amounts of crude oil/bitumens were also reduced by microorganisms during biodegradation. Jones et al. (2008) suggested that microorganisms can mineralize up to 60 wt% of a non-biodegraded oil. The major mass loss (~50%) of oils occurs from slight to moderate stages (PM level 1–4) through the removal of saturates, especially alkanes (Jones et al., 2008; Pan et al., 2017a). Further biodegradation (PM level 5–10) causes less mass loss (<20%) of oils by structural rearrangements (Head et al., 2003). Such significant mass loss at the low to moderate biodegradation stages, supplemented by the decrease in the hydrocarbon gas generation potential of the remaining reservoir oils, could significantly decrease secondary gas potential of oil reservoirs due to biodegradation.

Solid bitumen is another stable end-product of oil cracking under thermal stress. Wang et al. (2007) suggested that the solid bitumen yields correlate well with the hydrocarbon gas yields during the thermal cracking of oils, and the quantitative assessment of solid bitumen is useful in estimating the secondary gas potential in reservoirs. However, such correlations are subject to the severity of crud eoil biodegradation. Biodegradation reduces the hydrocarbon gas generation potential of residual oils while enhancing their solid bitumen yields under thermal stress (Fig. 4c,f). The solid bitumen yields from biodegraded bitumens can be 2–4 times that of the non-biodegraded oil in the EasyRo% range of 1.6–2.5% (Fig. 9a), but they decrease with increasing maturity. As a result, the non-biodegraded oil can produce 2–4 times the amount of of C_1–C_5 hydrocarbon gases while yielding the same amount of solid bitumen with the biodegraded bitumens in the EasyRo% range of 1.6–2.5% (Fig. 9b). Therefore, the biodegradation severity of precursor oils should be taken into consideration when correlating hydrocarbon gas resources with solid bitumens in secondary gas reservoirs. For example, the oil secondary cracking gas resource of the Anyue gas field may be significantly overestimated if only the amount of solid bitumen is taken into account but the biodegradation of crude oil in reservoir prior to secondary cracking is neglected. Additionally, the relationship between the amount of solid bitumen and oil secondary cracking gas yield might not only be influenced by biodegradation severity, but also by the initial composition of crude oil.

4.2. Hydrocarbon gas compositions and stable carbon isotopic compositions

In addition to the hydrocarbon gas generation potential, there are also variations in the chemical compositions of thermogenic hydrocarbons gases from different biodegraded oils. In the oil-generative window (EasyRo 0.7–1.3%), the thermogenic hydrocarbon gases from the oils with higher biodegradation severity (L-5 and L-8) were drier (i.e, relatively more enriched in methane) than those from the oils with lower biodegradation severity (L-0 and L-2) at the same thermal maturity (Fig. 10). The differences in the dryness of hydrocarbon gas from L-0, L-2, L-5, and L-8 became less significant when cracking of the C_2–C_5 gases became significant at the overmature stage (EasyRo > 2.0%).

Saturated hydrocarbons such as normal and branched alkanes are usually the primary source of C_2–C_5 gases during oil cracking. Tian et al. (2012) reported that the maximum C_2–C_5 gas yields from saturates can be over 400 mg/g, while those from aromatics and asphaltenes are both less than 200 mg/g. The cracking of alkanes to C_2–C_5 gases usually follows a C–C homolytic scission mechanism (Mango, 1990; Pepper and Corvi, 1995; Schenk et al., 1997; Zhang et al., 2008; Tian et al., 2009). The C_6–C_{13} alkanes can crack to C_2–C_5 gases step by step under thermal stress, while C_{14+} alkanes can simultaneously crack into C_6–C_{13} hydrocarbons (Hill et al., 2003), indirectly contributing to C_2–C_5 gas yields. The non-biodegraded
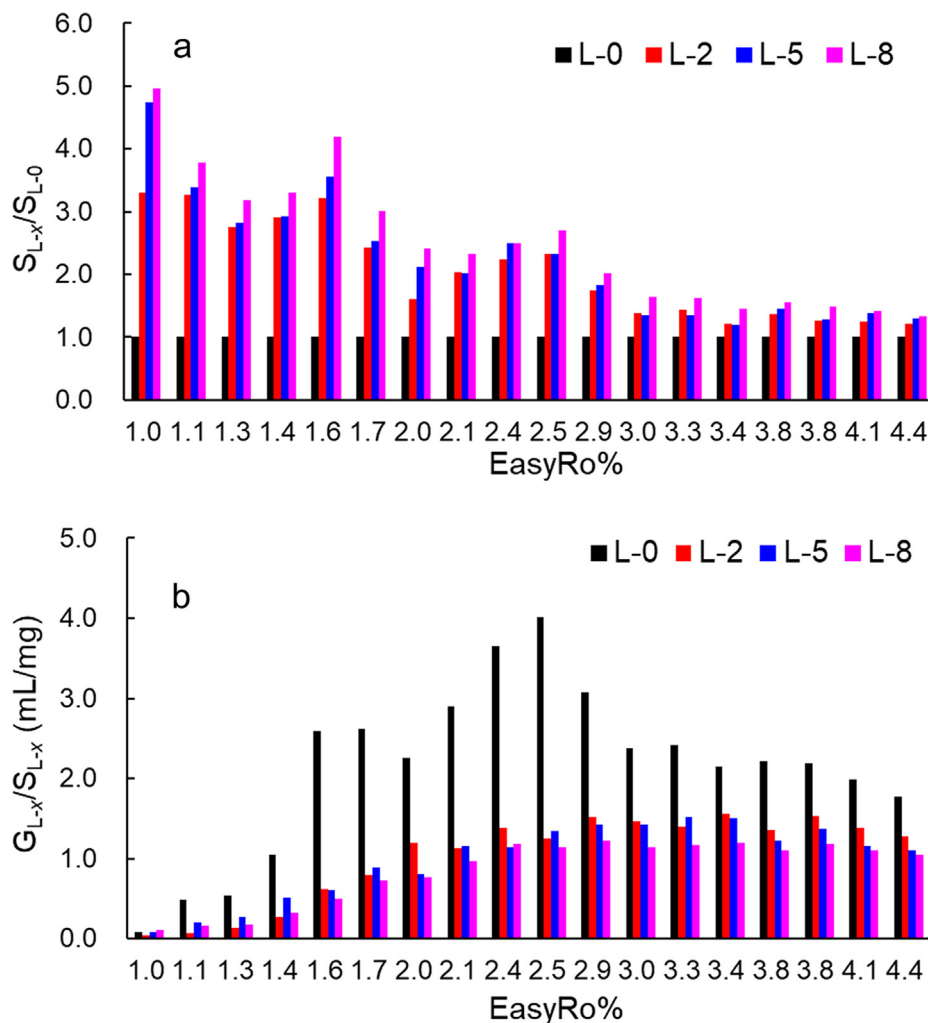
Fig. 9. (a) The ratios of solid bitumen yields from oil/bitumen L-x (x = 0, 2, 5, and 8) to solid bitumen yields from L-0; (b) the gas yield in volume normalized by the solid bitumen yield in weight for the four samples. S_{L-x} = solid bitumen yields from L-x (x = 0, 2, 5, and 8); G_{L-x} = gas yield from oil/bitumen L-x (x = 0, 2, 5, and 8) in volume.
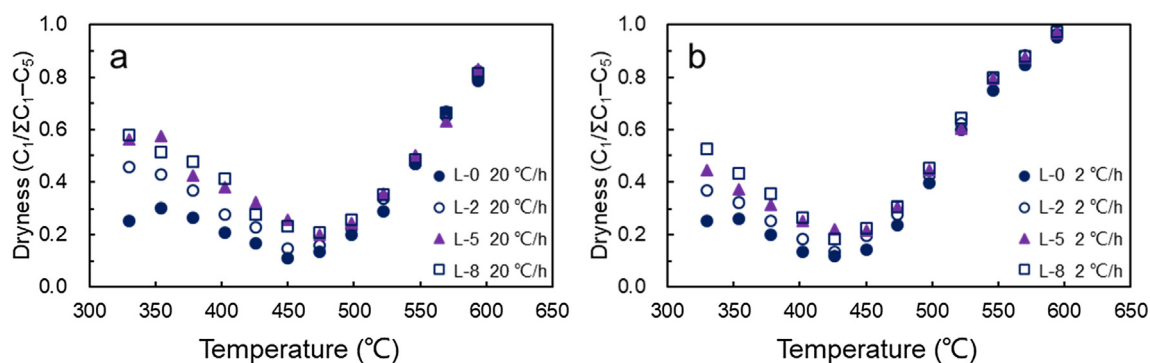
Fig. 10. Plots of gas dryness index ($C_1/\Sigma C_1$–C_5) vs pyrolysis temperatures at heating rates of 20 °C/h (a) and 2 °C/h (b), respectively.

oil L-0 contains abundant normal and branched alkanes with carbon numbers in the range of 11–37. Furthermore, the C_6–C_{13} yields from oil L-0 are also much higher than those from biodegraded oils at the same pyrolysis temperatures. As a result, more C_2–C_5 gases could be generated from the cracking of oil L-0 than those of the biodegraded oils. However, the C_6–C_{13} alkanes are usually susceptible to biodegradation and they were significantly removed at slight to moderate biodegradation. Therefore, the newly generated C_6–$C_{13}$ alkanes present in the pyrolysates of L-2 (Fig. 3) were mainly generated from the cracking of heavy fractions and residual C_{14+} alkanes, and thus their C_6–C_{13} alkane yields are lower than those of L-0. Consequently, the C_2–C_5 gas yields of L-2 are lower than those of L-0. Although L-5 and L-8 were depleted of alkanes during biodegradation, both C_6–C_{13} alkanes and C_{14+} alkanes were present in their pyrolysates (Fig. 3). This should be attributed to the release of aliphatic units from the molecular structure of aromatics, resins and asphaltenes (McKinney et al., 1998; Hill et al., 2003; Al Darouich et al., 2006; Behar et al., 2008). The relatively

lower amount of C_6–C_{13} alkanes and C_{14+} alkanes in the heavily biodegraded oils L-5 and severely biodegraded L-8 should be the main factors responsible for their relatively lower C_2–C_5 gas yields. In spite of varying gas sources, there was relatively small enrichment of ^{13}C (up to ~3.5‰ toward less negative δ^{13}C values) in the ethane generated from L-5 and L-8 compared to that from L-0 between EasyRo 0.9–1.6%. This is consistent with the work by Xiong and Geng (2000) in which asphaltene pyrolysates generated from the severely biodegraded oils exhibited n-alkane carbon isotopic compositions similar to that of non-biodegraded oil, with the n-alkanes in asphaltene pyrolysates generated from the severely biodegraded oils being slightly enriched in ^{13}C.

The methane generating mechanism is different from the generation of C_2–C_5 gases to some extent. Although the non-biodegraded oil L-0 contained abundant saturates, methane formation via terminal C–C cleavage or loss of methyl groups from saturated hydrocarbons requires higher activation energy than C–C homolytic scission (Hill et al., 2003; Zhang et al., 2008; Burklé-Vitzthum et al., 2011). Thus, it is not surprising that methane yields from L-0 below EasyRo ~ 0.7% is too low to accurately measure its carbon isotopes. By contrast, methyl groups attached to aromatic rings (α carbon) in aromatics, resins and asphaltenes are thermally less stable than alkyl carbons, and they can produce methane via demethylation reactions even in the oil-generative window (Behar et al., 1992, 1999; Killops et al., 1998; Lorant et al., 2000; Killops and Killops, 2005). For example, the work by Tian et al. (2012) suggested that aromatics and asphaltenes can produce more methane than saturates at less than 450 °C in the 2 °C/h run. As shown in Supplementary Fig. S1, there was no significant increase of methyl groups in asphaltene structure with increasing biodegradation severity. However, with the depletion of saturates during biodegradation, the aromatic structures in the aromatics, resins and asphaltenes became relatively enriched, likely leading to the relative enrichment of α carbonss. As a result, relatively higher methane yields may be generated from these α carbon through demethylation. That is, relatively higher methane yields can be generated from more severely biodegraded oils in the early oil-generative window due to the progressive enrichment of aromatics, resins and asphaltenes, which usually have more abundant α carbons. However, the maximum methane yield of crude oil should be subject to its hydrogen content. Since L-0 and L-2 are relatively more enriched in hydrogen, it is reasonable that the maximum methane yields of L-0 and L-2 exceeded those of L-5 and L-8 at the overmature stage (EasyRo > 2.0%).

With increasing thermal maturity, the stable carbon isotopic ratios of methane from biodegraded oils L-2, L-5 and L-8 first became enriched in ^{12}C and then in ^{13}C, consistent with previous observations (Lorant et al., 1998; Hill et al., 2003; Tian et al., 2012). This may suggest that there are several methane-generating precursors which have different carbon isotopic compositions. Liao et al. (2009) suggested that asphaltenes separated from Liaohe biodegraded oils are more enriched in ^{13}C than the corresponding saturates. Since n-C_{16}–n-C_{27} released from asphaltenes have similar carbon isotopic values with those in the saturates (Xiong and Geng, 2000), it is possible that the methyl groups in asphaltenes could be enriched in ^{13}C relative to the alkanes. The early release of these methyl groups via demethylation may result in the initial generation of ^{13}C-enriched methane. Therefore, in the more severely biodegraded oil, a larger portion of methane may be generated from these ^{13}C enriched methyl groups (especially from α carbons). This may explain the results that the methane generated from more severely biodegraded oils are significantly more enriched in ^{13}C (Fig. 6a, d) in the oil-generative window. It should be noted that demethylation of α carbons should only account for a small portion of the methane generation potential. With increasing thermal stress, methane generation from the cracking of saturates is enhanced. This should shift the thermogenic methane toward more negative isotopic values since saturates are more enriched in ^{12}C than the corresponding asphaltenes (Liao et al., 2009). Beyond the oil-generative window (EasyRo > 1.3%), the carbon isotopic ratios of methane from different biodegraded oils became rather close, with more severely biodegraded oils being enriched in ^{13}C (less than 3.1‰). Such differences may not only result from the carbon isotopic variations (up to 4.0‰ difference in δ^{13}C values) between the n-alkanes in non-biodegraded oil and those n-alkanes released from asphaltenes of biodegraded oils (Xiong and Geng, 2000; Sun et al., 2005), but also result from the differences in the content of residual alkanes that can crack into hydrocarbon gases.

Natural gases from different sources can sometimes be distinguished using gas compositions and/or stable carbon isotopic compositions, which may also be influenced by biodegradation. For example, the diagram of $\ln(C_1/C_2)$ vs $\ln(C_2/C_3)$ is usually employed to differentiate thermogenic gases sourced from oil cracking and kerogen cracking (Behar et al., 1992). Fig. 11a suggests that $\ln(C_1/C_2)$ is susceptible to biodegradation (Fig. 11a), increasing with increasing biodegradation, especially in the oil-generative window, while $\ln(C_2/C_3)$ is less susceptible to biodegradation (Fig. 11b). The
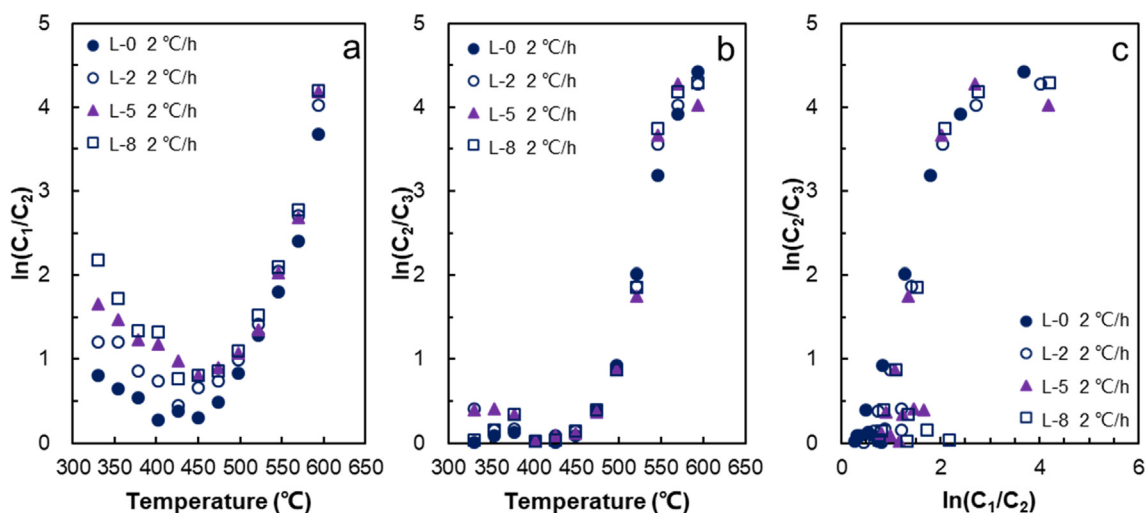
Fig. 11. Thermal evolution profiles of methane, ethane, and propane during pyrolysis in the experimental run of 2 °C/h. (a) Plot of $\ln(C_1/C_2)$ vs pyrolysis temperatures; (b) Plot of $\ln(C_2/C_3)$ vs pyrolysis temperatures; (c) Plot of $\ln(C_1/C_2)$ vs $\ln(C_2/C_3)$.
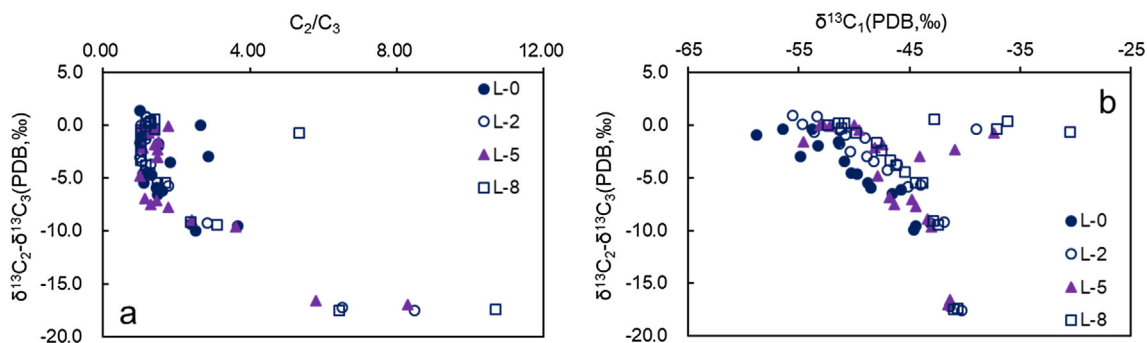
Fig. 12. Relationships between: (a) C_2/C_3 vs $\delta^{13}C_2-\delta^{13}C_3$ for gases from different biodegraded bitumens, and (b) $\delta^{13}C_1$ vs $\delta^{13}C_2-\delta^{13}C_3$ for gases from different biodegraded bitumens. Some data points that are present in (a) are missing in (b) due to the lack of $\delta^{13}C_1$ data.
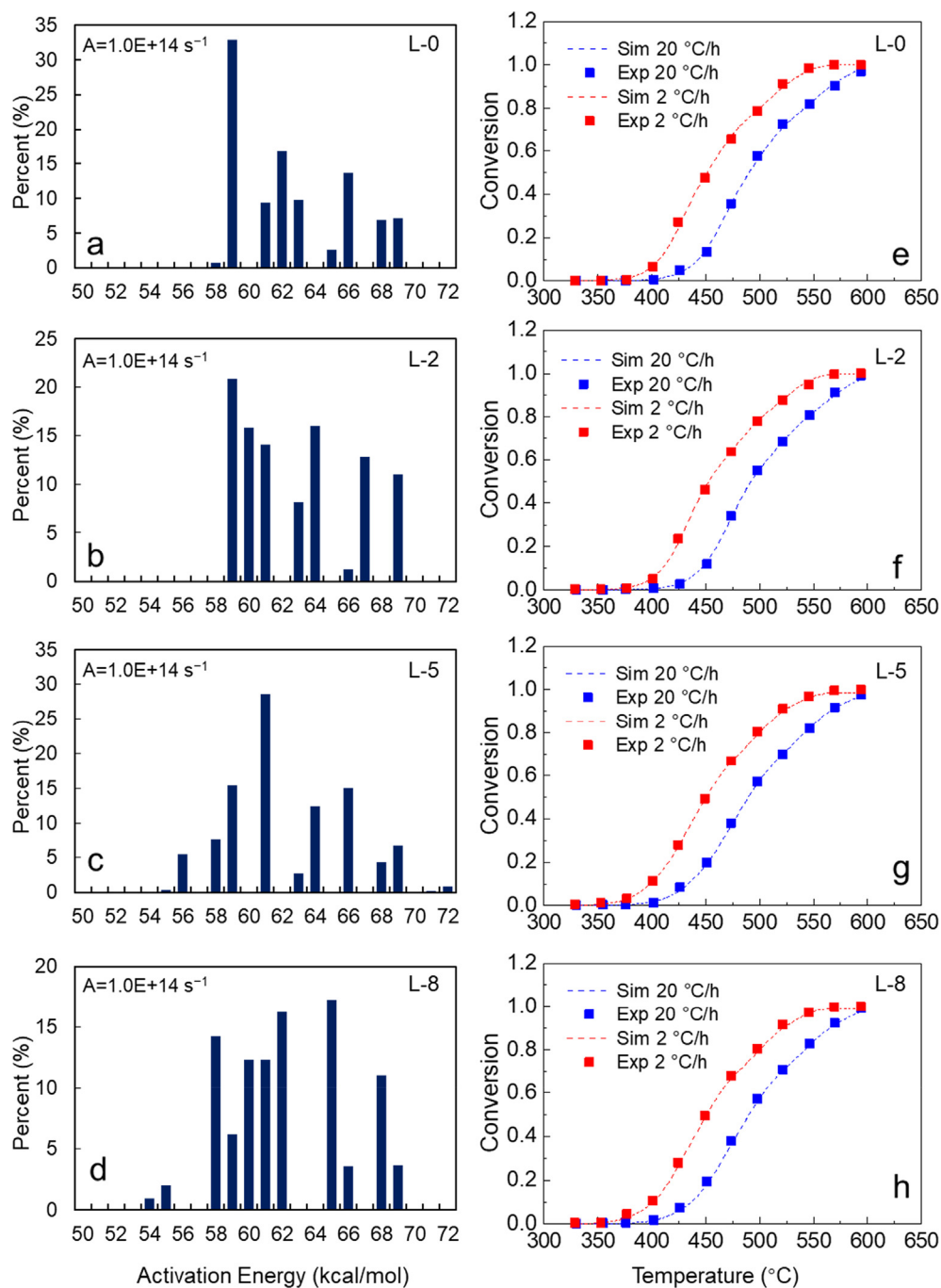
Fig. 13. The kinetic parameters (a, b, c and d) and modeling results (e, f, g, and h) for the bulk generation of C_1-C_5 gas from the pyrolysis of the four samples.

latter does not show systematic changes with biodegradation. Fig. 11c shows the diagram of $\ln(C_1/C_2)$ vs $\ln(C_2/C_3)$ of thermogenic gases from the four samples in this study. The biodegraded oils are located to the right side of the non-biodegraded oil. Nevertheless, the data points representing the non-biodegraded and biodegraded both follow a near vertical middle region followed by a region dominantly controlled by increasing $\ln(C_1/C_2)$. Such variation trends are similar to previous reports on oil cracking and they are different from the sub-horizontal trend in the diagram of $\ln(C_1/C_2)$ vs $\ln(C_2/C_3)$ generated from kerogen cracking gases (Behar et al., 1992; Prinzhofer and Huc, 1995).

The diagram of $\delta^{13}C_2 - \delta^{13}C_3$ vs C_2/C_3 and the plot of $\delta^{13}C_1$ vs $\delta^{13}C_2 - \delta^{13}C_3$ has been proposed to distinguish secondary gas from that generated directly by kerogen (Prinzhofer and Huc, 1995; Guo et al., 2009). Tian et al. (2012) further suggested that gases from different SARA fractions of crude oil have different trends on the plot of $\delta^{13}C_2 - \delta^{13}C_3$ vs C_2/C_3. In this study, although the saturates was preferentially consumed with increasing biodegradation, there is no significant systematic variation in either C_2/C_3 or $\delta^{13}C_2 - \delta^{13}C_3$ (Fig. 12a). The $\delta^{13}C_2 - \delta^{13}C_3$ vs C_2/C_3 diagram can be applied to evaluate the origin of reservoir gases in superimposed basins in spite of the preceding in-reservoir biodegradation. However, it seems biodegradation can affect the plot of $\delta^{13}C_1$ vs $\delta^{13}C_2 - \delta^{13}C_3$ (Fig. 12b). Fig. 6 and Fig. 12b indicate that the methane generated from the biodegraded bitumens L-2, L-5 and L-8 is less enriched in ^{12}C than that from the non-biodegraded oil L-0, resulting in the formers significant positive shift of the curve.

4.3. Kinetic modeling and geological implications

Assuming that oil cracking consists of multiple parallel first-order reactions, the non-isothermal pyrolysis data obtained in this study were employed to determine the kinetic parameters of the four samples by curve fitting. A fixed frequency factor $(1.0 \times 10^{-14} \text{ s}^{-1})$ was imposed on the four samples for comparison purposes. Fig. 13 shows the kinetic modeling results for the bulk generation of C_1-C_5 gases (vol/wt) for the four samples. There are differences in the activation energy distributions of the four samples. L-0 and L-2 have a relatively concentrated distribution of activation energy in the range of 58–69 kcal/mol. In contrast, the activation energy distributions of L-5 and L-8 cover wider ranges, with an increasing proportion of initial potential with low activation energy. This suggests that biodegradation of moderate/severe stage can increase the heterogeneity of residual oils. The increasing proportion of lower activation energy in L-5 and L-8 is likely attributed to the increasing content of heavy fractions, especially asphaltenes, in these biodegraded bitumens and associated with α-methyl cleavage from aromatic moieties.

The kinetic parameters above have been extrapolated to geological conditions of 2 °C/Ma with an initial temperature of 50 °C (Fig. 14). The maximum C_1-C_5 hydrocarbon gas yields are similar for L-5 and L-8, both of which are lower than the maximum C_1-C_5 hydrocarbon gas yields from L-0 and L-2. The result suggests that failing to consider the influence of biodegradation in a biodegraded reservoir could result in overestimation of the gas resource. Nevertheless, L-5 and L-8 begin to generate hydrocarbon gases earlier than L-0 and L-2. When the yield of C_1-C_5 gases reaches 5 mL/g, the required temperature of L-5 is about 151 °C whereas that of L-0 is about 163 °C. The C_1-C_5 hydrocarbon gas yields from L-0 do not exceed those from L-5 until the formation temperature reaches 184 °C (EasyRo = 1.68%), which is close to the predicted temperature where the C_1-C_5 gas yield from crude oil exceeds that of asphaltenes in Tian et al. (2012). Therefore, biodegradation of moderate/severe stage oils can decrease the thermal stability of residual oils, promoting oil transformation and early generation of hydrocarbon gases. Such influences should be considered
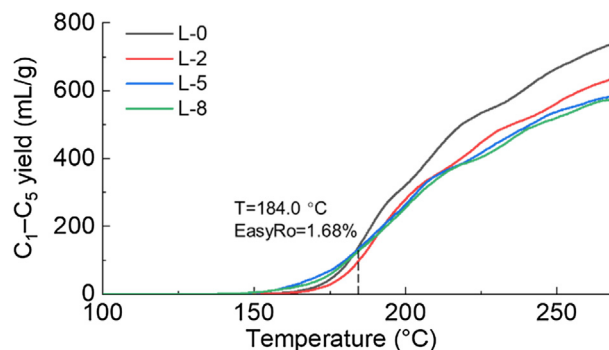

Fig. 14. The amounts of total C_1-C_5 gases by volume for the four samples modeled under geological conditions of 2 °C/Ma and an initial temperature of 50 °C.

in the exploration of biodegraded reservoirs to avoid the underestimation of the degree of oil transformation. However, the magnitude of such influence may not only be controlled by biodegradation severity, but also by the initial composition of crude oil, especially alkanes.

5. Conclusions

Biodegradation preferentially removed the hydrogen-rich species in crude oils, such as normal and branched alkanes, and thus could reduce the secondary gas generation potential of crude oils. The decrease in the hydrocarbon gas generation potential became insignificant after the complete removal of normal and branched alkanes. Furthermore, biodegraded oils can yield more solid bitumen than non-biodegraded oil while producing the same amount of hydrocarbon gases. This may lead to overestimation of hydrocarbon gas resources generated through secondary cracking of biodegraded oils by the quantitative assessment of solid bitumens in reservoirs. Moreover, the thermogenic hydrocarbon gases from the non-biodegraded oil and biodegraded oils are different in their chemical compositions and carbon isotopic compositions, and the thermogenic hydrocarbon gases from the more severely biodegraded oils are drier and more enriched in ^{13}C, especially in the oil-generative window. Such differences become smaller with increasing thermal stress above the oil-generative window. The kinetic modeling results show that moderately and severely biodegraded oils begin to thermally decompose at lower temperatures than that of non-biodegraded and slightly biodegraded oils. The hydrocarbon generation of moderately and severely biodegraded oils starts earlier than that of non-biodegraded and slightly biodegraded oils.

Declaration of Competing Interest

The authors declare that they have no known competing financial interests or personal relationships that could have appeared to influence the work reported in this paper.

Appendix A. Supplementary material

Supplementary data to this article can be found online at https://doi.org/10.1016/j.orggeochem.2019.103965.

Associate Editor—**Lloyd Snowdon**

References

Aitken, C.M., Jones, D.M., Larter, S.R., 2004. Anaerobic hydrocarbon biodegradation in deep subsurface oil reservoirs. Nature 431, 291–294.

Al Darouich, T., Behar, F., Largeau, C., 2006. Thermal cracking of the light aromatic fraction of Safaniya crude oil – experimental study and compositional modeling of molecular classes. Organic Geochemistry 37, 1130–1154.

Behar, F., Budzinski, H., Vandenbroucke, M., Tang, Y., 1999. Methane generation from oil cracking: Kinetics of 9-methylphenanthrene cracking and comparison with other pure compounds and oil fractions. Energy & Fuels 13, 471–481.

Behar, F., Kressmann, S., Rudkiewicz, J.L., Vandenbroucke, M., 1992. Experimental simulation in a confined system and kinetic modeling of kerogen and oil cracking. Organic Geochemistry 19, 173–189.

Behar, F., Lorant, F., Mazeas, L., 2008. Elaboration of a new compositional kinetic schema for oil cracking. Organic Geochemistry 39, 764–782.

Behar, F., Vandenbroucke, M., Tang, Y., Marquis, F., Espitalié, J., 1997. Thermal cracking of kerogen in open and closed systems: determination of kinetic parameters and stoichiometric coefficients for oil and gas generation. Organic Geochemistry 26, 321–339.

Burklé-Vitzthum, V., Bounaceur, R., Marquaire, P.-M., Montel, F., Fusetti, L., 2011. Thermal evolution of *n*- and *iso*-alkanes in oils. Part 1: Pyrolysis model for a mixture of 78 alkanes (C_1–C_{32}) including 13,206 free radical reactions. Organic Geochemistry 42, 439–450.

Calemma, V., Rausa, R., 1997. Thermal decomposition behavior and structural characteristics of asphaltenes. Journal of Analytical and Applied Pyrolysis 40, 569–584.

Chang, X., Zhao, H., He, W., Xu, Y., Xu, Y., Wang, Y., 2018. Improved understanding of the alteration of molecular compositions by severe to extreme biodegradation: a case study from the Carboniferous oils in the eastern Chepaizi uplift, Junggar Basin, Northwest China. Energy & Fuels 32, 7557–7568.

Chen, S., Zhu, Y., Wang, H., Liu, H., Wei, W., Fang, J., 2011. Shale gas reservoir characterization: a typical case in the southern Sichuan Basin of China. Energy 36, 6609–6616.

Chen, Z., Simoneit, B.R., Wang, T.-G., Yang, Y., Ni, Z., Cheng, B., Luo, B., Yang, C., Chen, T., 2017. Biomarker signatures of Sinian bitumens in the Moxi-Gaoshiti Bulge of Sichuan Basin, China: Geological significance for paleo-oil reservoirs. Precambrian Research 296, 1–19.

Cheng, B., Liao, Z., Wang, T., Liu, H., Tian, Y., Yang, S., 2015. Multiple charges to Sinian reservoirs in the middle Sichuan basin, SW China: Insight from the adsorbed/occluded hydrocarbons in solid bitumens. Journal of Petroleum Science and Engineering 127, 359–366.

Cheng, X., Hou, D., Xu, C., Wang, F., 2016. Biodegradation of tricyclic terpanes in crude oils from the Bohai Bay Basin. Organic Geochemistry 101, 11–21.

Connan, J., Le Tran, K., van der Weide, B., 1975. Alteration of petroleum in reservoirs. In: Ninth World Petroleum Congress Proceedings, Tokyo. Applied Science Publications, London, pp. 171–178

Cubitto, M.A., Morán, A.C., Commendatore, M., Chiarello, M.N., Baldini, M.D., Siñeriz, F., 2004. Effects of *Bacillus subtilis* O9 biosurfactant on the bioremediation of crude oil-polluted soils. Biodegradation 15, 281–287.

da Cruz, G.F., de Vasconcellos, S.P., Angolini, C.F., Dellagnezze, B.M., Garcia, I.N., de Oliveira, V.M., dos Santos Neto, E.V., Marsaioli, A.J., 2011. Could petroleum biodegradation be a joint achievement of aerobic and anaerobic microorganisms in deep-sea reservoirs?. AMB Express 1, 47.

Dutta, T.K., 2005. Origin, occurrence, and biodegradation of long-side-chain alkyl compounds in the environment: a review. Environmental Geochemistry and Health 27, 271–284.

Frontera-Suau, R., Bost, F.D., McDonald, T.J., Morris, P.J., 2002. Aerobic biodegradation of hopanes and other biomarkers by crude oil-degrading enrichment cultures. Environmental Science & Technology 36, 4585–4592.

Fusetti, L., Behar, F., Bounaceur, R., Marquaire, P.-M., Grice, K., Derenne, S., 2010. New insights into secondary gas generation from the thermal cracking of oil: Methylated monoaromatics. A kinetic approach using 1,2,4-trimethylbenzene. Part I: A mechanistic kinetic model. Organic Geochemistry 41, 146–167.

Guo, L., Xiao, X., Tian, H., Song, Z., 2009. Distinguishing gases derived from oil cracking and kerogen maturation: Insights from laboratory pyrolysis experiments. Organic Geochemistry 40, 1074–1084.

Head, I.M., Jones, D.M., Larter, S.R., 2003. Biological activity in the deep subsurface and the origin of heavy oil. Nature 426, 344.

Hill, R.J., Tang, Y., Kaplan, I.R., 2003. Insights into oil cracking based on laboratory experiments. Organic Geochemistry 34, 1651–1672.

Huang, H., Bowler, B.F.J., Zhang, Z., Oldenburg, T.B.P., Larter, S.R., 2003. Influence of biodegradation on carbazole and benzocarbazole distributions in oil columns from the Liaohe basin, NE China. Organic Geochemistry 34, 951–969.

Huang, H., Bowler, B.F.J., Oldenburg, T.B.P., Larter, S.R., 2004a. The effect of biodegradation on polycyclic aromatic hydrocarbons in reservoired oils from the Liaohe basin, NE China. Organic Geochemistry 35, 1619–1634.

Huang, H., Larter, S.R., Bowler, B.F., Oldenburg, T.B., 2004b. A dynamic biodegradation model suggested by petroleum compositional gradients within reservoir columns from the Liaohe basin, NE China. Organic Geochemistry 35, 299–316.

Jenisch-Anton, A., Adam, P., Michaelis, W., Connan, J., Herrmann, D., Rohmer, M., Albrecht, P., 2000. Molecular evidence for biodegradation of geomacromolecules. Geochimica et Cosmochimica Acta 64, 3525–3537.

Jin, M., Cao, J., Shi, C., Zeng, W., Shen, C., Shi, K., Cheng, X., Tan, X., 2016. Hydrocarbon origin and reservoir forming model research of Longwangmiao Formation, Moxi-Gaoshiti area, Sichuan Basin. Petroleum 2, 130–137.

Jones, D.M., Head, I.M., Gray, N.D., Adams, J.J., Rowan, A.K., Aitken, C.M., Bennett, B., Huang, H., Brown, A., Bowler, B.F.J., Oldenburg, T., Erdmann, M., Larter, S.R., 2008. Crude-oil biodegradation via methanogenesis in subsurface petroleum reservoirs. Nature 451, 176–180.

Killops, S., Funnell, R., Suggate, R., Sykes, R., Peters, K., Walters, C., Woolhouse, A., Weston, R., Boudou, J.-P., 1998. Predicting generation and expulsion of paraffinic oil from vitrinite-rich coals. Organic Geochemistry 29, 1–21.

Killops, S., Killops, V., 2005. Introduction to Organic Geochemistry. .

Larter, S., Huang, H., Adams, J., Bennett, B., Jokanola, O., Oldenburg, T., Jones, M., Head, I., Riediger, C., Fowler, M., 2006. The controls on the composition of biodegraded oils in the deep subsurface: Part II—Geological controls on subsurface biodegradation fluxes and constraints on reservoir-fluid property prediction. American Association of Petroleum Geologists Bulletin 90, 921–938.

Larter, S., Wilhelms, A., Head, I., Koopmans, M., Aplin, A., di Primio, R., Zwach, C., Erdmann, M., Telnaes, N., 2003. The controls on the composition of biodegraded oils in the deep subsurface—part 1: biodegradation rates in petroleum reservoirs. Organic Geochemistry 34, 601–613.

Leahy, J.G., Colwell, R.R., 1990. Microbial degradation of hydrocarbons in the environment. Microbiology and Molecular Biology Reviews 54, 305–315.

Li, D., 1996. Basic characteristics of oil and gas basins in China. Journal of Southeast Asian Earth Sciences 13, 299–304.

Liao, Y., Geng, A., Huang, H., 2009. The influence of biodegradation on resins and asphaltenes in the Liaohe Basin. Organic Geochemistry 40, 312–320.

Liao, Y., Shi, Q., Hsu, C.S., Pan, Y., Zhang, Y., 2012. Distribution of acids and nitrogen-containing compounds in biodegraded oils of the Liaohe Basin by negative ion ESI FT-ICR MS. Organic Geochemistry 47, 51–65.

Liao, Y., Zheng, Y., Pan, Y., Sun, Y., Geng, A., 2015. A method to quantify C_1–C_5 hydrocarbon gases by kerogen primary cracking using pyrolysis gas chromatography. Organic Geochemistry 79, 49–55.

Liu, W., Liao, Y., Pan, Y., Jiang, B., Zeng, Q., Shi, Q., Hsu, C.S., 2018. Use of ESI FT–ICR MS to investigate molecular transformation in simulated aerobic biodegradation of a sulfur-rich crude oil. Organic Geochemistry 123, 17–26.

Lorant, F., Behar, F., Vandenbroucke, M., McKinney, D.E., Tang, Y., 2000. Methane generation from methylated aromatics: kinetic study and carbon isotope modeling. Energy & Fuels 14, 1143–1155.

Lorant, F., Prinzhofer, A., Behar, F., Huc, A.Y., 1998. Carbon isotopic and molecular constraints on the formation and the expulsion of thermogenic hydrocarbon gases. Chemical Geology 147, 249–264.

Lu, S., He, W., Huang, H., 1990. The geochemical characteristics of heavy oil and its recovery in Liaohe Basin, China. Organic Geochemistry 16, 437–449.

Mango, F.D., 1990. The origin of light hydrocarbons in petroleum: a kinetic test of the steady-state catalytic hypothesis. Geochimica et Cosmochimica Acta 54, 1315–1323.

McKinney, D., Behar, F., Hatcher, P., 1998. Reaction kinetics and *n*-alkane product profiles from the thermal degradation of ^{13}C-labeled n-C_{25} in two dissimilar oils as determined by SIM/GC/MS. Organic Geochemistry 29, 119–136.

Moldowan, J.M., McCaffrey, M.A., 1995. A novel microbial hydrocarbon degradation pathway revealed by hopane demethylation in a petroleum reservoir. Geochimica et Cosmochimica Acta 59, 1891–1894.

Niu, J., Hu, J., 1999. Formation and distribution of heavy oil and tar sands in China. Marine and Petroleum Geology 16, 85–95.

Pan, Y., Liao, Y., Shi, Q., 2017a. Variations of acidic compounds in crude oil during simulated aerobic biodegradation: Monitored by semiquantitative negative-Ion ESI FT-ICR MS. Energy & Fuels 31, 1126–1135.

Pan, Y., Liao, Y., Sun, Y., 2017b. The characteristics of bound biomarkers released from asphaltenes in a sequence of naturally biodegraded oils. Organic Geochemistry 111, 56–66.

Pan, Y., Liao, Y., Zheng, Y., 2015. Effect of biodegradation on the molecular composition and structure of asphaltenes: Clues from quantitative Py–GC and THM–GC. Organic Geochemistry 86, 32–44.

Pang, X., Meng, Q., Jiang, Z., Liu, L., Lü, X., 2010. A hydrocarbon enrichment model and prediction of favorable accumulation areas in complicated superimposed basins in China. Petroleum Science 7, 10–19.

Pepper, A.S., Corvi, P.J., 1995. Simple kinetic models of petroleum formation. Part I: oil and gas generation from kerogen. Marine and Petroleum Geology 12, 291–319.

Peters, K.E., Walters, C.C., Moldowan, J.M., 2005. The Biomarker Guide. Cambridge University Press.

Prinzhofer, A.A., Huc, A.Y., 1995. Genetic and post-genetic molecular and isotopic fractionations in natural gases. Chemical Geology 126, 281–290.

Schenk, H.J., Di Primio, R., Horsfield, B., 1997. The conversion of oil into gas in petroleum reservoirs. Part 1: Comparative kinetic investigation of gas generation from crude oils of lacustrine, marine and fluviodeltaic origin by programmed-temperature closed-system pyrolysis. Organic Geochemistry 26, 467–481.

Setti, L., Lanzarini, G., Pifferi, P.G., Spagna, G., 1993. Further research into the aerobic degradation of n-alkanes in a heavy oil by a pure culture of a Pseudomonas sp. Chemosphere 26, 1151–1157.

Shi, C., Cao, J., Tan, X., Luo, B., Zeng, W., Hu, W., 2017. Discovery of oil bitumen co-existing with solid bitumen in the Lower Cambrian Longwangmiao giant gas reservoir, Sichuan Basin, southwestern China: Implications for hydrocarbon accumulation process. Organic Geochemistry 108, 61–81.

Sun, Y., Chen, Z., Xu, S., Cai, P., 2005. Stable carbon and hydrogen isotopic fractionation of individual n-alkanes accompanying biodegradation: evidence from a group of progressively biodegraded oils. Organic Geochemistry 36, 225–238.

Sun, L., Jiang, T., Xu, H., Shan, J., Lian, Z., 2009. Unsteady reservoir in Hadson Oilfield, Tarim Basin. Petroleum Exploration and Development 36, 62–67.

Sun, Y., Jin, Y., Gu, Q., Shen, Y., Yang, F., 2003. Timing of paleo-oil accumulation in Tadong No. 2 Well, Tarim Basin. Petroleum Exploration and Development 30, 31–33.

Sweeney, J.J., Burnham, A.K., 1990. Evaluation of a simple model of vitrinite reflectance based on chemical kinetics. American Association of Petroleum Geologists Bulletin 74, 1559–1570.

Tang, Y., Zan, L., 2009. Molecular fossils and sources of Cambrian heavy oil of Well Tadong-2 in the Tarim Basin, Xinjiang, China. Chinese Journal of Geochemistry 28, 314–319.

Tian, H., Xiao, X., Yang, L., Xiao, Z., Guo, L., Shen, J., Lu, Y., 2009. Pyrolysis of oil at high temperatures: Gas potentials, chemical and carbon isotopic signatures. Chinese Science Bulletin 54, 1217–1224.

Tian, H., Xiao, X., Wilkins, R.W.T., Tang, Y., 2012. An experimental comparison of gas generation from three oil fractions: Implications for the chemical and stable carbon isotopic signatures of oil cracking gas. Organic Geochemistry 46, 96–112.

Volkman, J.K., Alexander, R., Kagi, R.I., Rowland, S.J., Sheppard, P.N., 1984. Biodegradation of aromatic hydrocarbons in crude oils from the Barrow Sub-basin of Western Australia. Organic Geochemistry 6, 619–632.

Wang, T., Geng, A., Li, X., 2010. Pyrolysis of one crude oil and its asphaltenes: evolution of gaseous hydrocarbons and carbon isotope. Journal of Petroleum Science and Engineering 71, 8–12.

Wang, T., Geng, A., Xiong, Y., Geng, X., 2007. Mass balance calculation of the pyrolysates generated from marine crude oil: A prediction model of oil cracking gas resources based on solid bitumen in reservoir. Chinese Science Bulletin 52, 1532–1539.

Wang, Y., Zhang, S., Wang, F., Wang, Z., Zhao, C., Wang, H., Liu, J., Lu, J., Geng, A., Liu, D., 2006. Thermal cracking history by laboratory kinetic simulation of Paleozoic oil in eastern Tarim Basin, NW China, implications for the occurrence of residual oil reservoirs. Organic Geochemistry 37, 1803–1815.

Watson, J.S., Jones, D.M., Swannell, R.P.J., van Duin, A.C.T., 2002. Formation of carboxylic acids during aerobic biodegradation of crude oil and evidence of microbial oxidation of hopanes. Organic Geochemistry 33, 1153–1169.

Wei, G., Chen, G., Du, S., Zhang, L., Yang, W., 2008. Petroleum systems of the oldest gas field in China: Neoproterozoic gas pools in the Weiyuan gas field, Sichuan Basin. Marine and Petroleum Geology 25, 371–386.

Wei, G., Xie, Z., Song, J., Yang, W., Wang, Z., Li, J., Wang, D., Li, Z., Xie, W., 2015. Features and origin of natural gas in the Sinian-Cambrian of central Sichuan paleo-uplift, Sichuan Basin, SW China. Petroleum Exploration and Development 42, 768–777.

Wentzel, A., Ellingsen, T.E., Kotlar, H.-K., Zotchev, S.B., Throne-Holst, M., 2007. Bacterial metabolism of long-chain n-alkanes. Applied Microbiology and Biotechnology 76, 1209–1221.

Xiong, Y., Geng, A., 2000. Carbon isotopic composition of individual n-alkanes in asphaltene pyrolysates of biodegraded crude oils from the Liaohe Basin, China. Organic Geochemistry 31, 1441–1449.

Yuan, H., Xu, G., Wang, G., Mao, M., Liang, J., 2009. Phase evolution during hydrocarbon accumulation and exploration prospect for Sinian reservoirs in central Sichuan basin, China. Journal of Chengdu University of Technology 36, 662–668 (in Chinese with English abstract).

Xiong, Y., Jiang, W., Wang, X., Li, Y., Chen, Y., Zhang, L., Lei, R., Peng, P., 2016. Formation and evolution of solid bitumen during oil cracking. Marine and Petroleum Geology 78, 70–75.

Zhang, H., Geng, A., Xiong, Y., Liu, J., Liu, J., 2008. Closed-system programmed-temperature pyrolysis on n-octadecane: Implications for the conversion of oil to gas. Geochemical Journal 42, 403–412.

Zhang, Q., Huang, H., Zheng, L., Qin, J., 2007a. Secondary hydrocarbon generation potential from heavy oil, oil sand and solid bitumen during the artificial maturation. Organic Geochemistry 38, 2024–2035.

Zhang, S., Wang, Z., Wang, F., Liang, D., 2004. Oil accumulation history in Tadong 2 oil reservoir in Tarim Basin, NW China—A case study of oil stability and cracking. Petroleum Exploration and Development 31, 25–30.

Zhang, S., Liang, D., Zhu, G., Zhang, X., Zhang, B., Chen, J., Zhang, B., 2007b. Fundamental geological elements for the occurrence of Chinese marine oil and gas accumulations. Chinese Science Bulletin 52, 28–43.

Zhang, Z., Hou, Z., Yang, C., Ma, C., Tao, F., Xu, P., 2011. Degradation of n-alkanes and polycyclic aromatic hydrocarbons in petroleum by a newly isolated Pseudomonas aeruginosa DQ8. Bioresource Technology 102, 4111–4116.

Zhao, W., Hu, S., Liu, W., Wang, T., Jiang, H., 2015. The multi-staged "golden zones" of hydrocarbon exploration in superimposed petroliferous basins of onshore China and its significance. Petroleum Exploration and Development 42, 1–13.

Zhu, G., Wang, T., Xie, Z., Xie, B., Liu, K., 2015. Giant gas discovery in the Precambrian deeply buried reservoirs in the Sichuan Basin, China: implications for gas exploration in old cratonic basins. Precambrian Research 262, 45–66.

Zou, C., Du, J., Xu, C., Wang, Z., Zhang, B., Wei, G., Wang, T., Yao, G., Deng, S., Liu, J., Zhou, H., Xu, A., Yang, Z., Jiang, H., Gu, Z., 2014. Formation, distribution, resource potential, and discovery of Sinian-Cambrian giant gas field, Sichuan Basin, SW China. Petroleum Exploration and Development 41, 306–325.